The Effect of Mixer Properties and Fill Level on Granular Flow in a Bladed Mixer

Brenda Remy and Benjamin J. Glasser
Dept. of Chemical and Biochemical Engineering, Rutgers University, Piscataway, NJ, 08854

Johannes G. Khinast
Institute for Process Engineering, Graz University of Technology, Inffeldgasse 21/A, Graz, A-8010, Austria

DOI 10.1002/aic.11979
Published online October 23, 2009 in Wiley InterScience (www.interscience.wiley.com).

The discrete element method was used to study the effect of mixer properties and fill level on the granular flow of monodisperse, cohesionless spheres in a bladed mixer. For fill levels just covering the span of the blades, a three-dimensional (3-D) recirculation zone develops in front of the blades, which promotes vertical and radial mixing. Increasing fill level reduces the size of the recirculation zone, decreases bed dilation and hinders particle diffusivities. However, above a critical fill level, the behavior of the particles within the span of the blade is found to be invariant of fill level. At low-fill levels, the pressure within the particle bed varies linearly with bed height and can be approximated by hydrostatics. At higher fill levels, a constant pressure region develops within the span of the blades due to the angled pitch of the blades. Cylinder wall friction is shown to significantly influence granular behavior in bladed mixers. At low-wall friction, the 3-D recirculation zone observed for high-wall friction conditions does not develop. High-wall friction leads to an increase in convective and diffusive particle mixing. Shear stresses are shown to be a function of wall friction. Blade position along the vertical axis is shown to influence flow patterns, granular temperature and stress. The effect of increasing the mixer diameter at a constant particle diameter was also studied. When the mixer diameter is larger than a critical size such that wall effects are minimized, the observed granular behavior follows simple scaling relations. Particle velocities and diffusivities scale linearly with mixer size and blade speed. Normal and shear stress profiles are found to scale linearly with the total weight of the particle bed. © 2009 American Institute of Chemical Engineers *AIChE J,* 56: 336–353, 2010
Keywords: bladed mixer, DEM, granular mixing, scale-up and quasi-static flows

Introduction

Many industrial processes involving granular materials employ the use of mixers with mechanical agitators that provide shear, induce flow and encourage mixing. The appeal of these mixers comes from their ability to handle a wide variety of solids ranging from free flowing to cohesive powders and even pastes.[1] Mixer characteristics such as shape, size and agitator configuration determine the flow patterns, degree of mixing and the shear profile achieved in such devices.[2,3] The agitator configuration often dictates the type of mixing patterns obtained and the amount of momentum transferred to the particle bed. The size and shape of the mixer could promote or inhibit the development of mixing dead zones,[4] or the tendency for flow stoppage or segregation to occur.[5] In addition to mixer properties, operating conditions, such as fill level, have been shown to significantly affect the flow behavior in agitated devices.[6–9] Mixer fill level could influence the size of recirculation zones, particle velocities, and bed turnover rate and particle dispersion.

Correspondence concerning this article should be addressed to B. J. Glasser at bglasser@rutgers.edu

Changes in fill level could even lead to flow regime changes at constant agitator speeds.

Although equipment geometry and operating parameters play an important role, currently it is difficult — if not impossible — to predict granular behavior in mechanically agitated beds when these attributes are changed. Often during the early stages of process development and design, laboratory or pilot plant experiments are carried out with different equipment configurations, at smaller scales or at different fill levels than what will ultimately be used at the manufacturing scale. The uncertainty surrounding the effects of mixer properties on granular flows opens up the door for complications to occur during scale-up, which may not be easily explained or prevented. Thus, understanding the role of mixer parameters and operating conditions in agitated devices is critical for designing and engineering reliable processes.

In this work, we studied the effect of mixer properties and fill level on granular flows in a cylindrical mixer mechanically agitated by an impeller with four blades pitched at a 45° angle using the discrete element method. Our mixer geometry is representative of several industrial granular processes, including filter dryers and high-shear granulators. Granular flows in this type of mixer have been recently studied by various investigators experimentally,[10–12] and via computer simulations.[13–17] The work done thus far has provided an initial understanding of granular behavior in bladed mixers. However, most of these studies have focused on the effect of particle properties on granular flow and segregation for a limited range of process conditions. None of these studies have examined the effect of mixer parameters on the observed granular behavior. Thus, the role of mixer properties on the resulting granular flows is not well understood. Additionally, fill levels covering just the top of the blades have mostly been used. Bladed mixers at the industrial scale are usually operated at much higher fill levels to increase equipment productivity. Only Stewart et al.[12] studied the influence of fill level on a flat-bladed mixer. They showed that fill level affects bed dilation, particle velocities and flow patterns. The effect of fill level in more complex blade configurations remains to be studied.

The discrete element method (DEM) has become an important tool in the study of granular flows. This technique provides insight into the system's dynamics and transient behavior, and allows for the study of parameters that are difficult to measure or vary experimentally. For example, DEM simulations provide information on localized flow, contact network structures and stress profiles; parameters that with current experimental techniques are difficult if not impossible to obtain. Several researchers in the past have shown the ability of DEM simulations to capture accurately particulate flows and bulk behavior in a variety of systems[18–22] including bladed mixers[17] when compared to experimental results. While DEM has proven to be a reliable tool, the number of particles that can be examined with DEM is limited by computer processing power. Most of the DEM work thus far has been performed with systems of $\sim 10^5$ particles, while industrial processes operate with systems of more than 10^{10} particles.[23] It remains uncertain whether the results obtained with the smaller systems can be extended to the larger scale, industrial systems. Knowledge of how system size affects the bulk behavior of granular materials is necessary for the development of first principles-based scale-up approaches.

The goal of this study is to provide a 3-D picture of granular behavior when mixer characteristics, such as particle-wall friction, blade position, mixer diameter to particle diameter and fill level, are changed. Previous numerical results have shown that that the frictional characteristics of the particle bed strongly influence the granular behavior observed in bladed mixers[14,15] However, in these studies, the frictional characteristics of the particle-boundary interactions were not varied from those of the particle–particle interactions. Currently it is unknown whether a change in the particle-boundary friction will lead to a change in granular behavior. The effect of changing this parameter might become important during scale-up, since often the material of construction of the laboratory scale mixer differs from that of the manufacturing scale unit. The blade position relative to the mixer height is often changed in bladed mixers at the industrial level to enhance mixing at higher fill levels. The influence of blade position in a bladed mixer has also remained unstudied. The ratio of mixer diameter to particle diameter has been shown to be an important parameter in other granular processes such as rotating drums.[24–26] The previous bladed mixers studies were performed while keeping this ratio a constant. This ratio is one of the parameters that changes when bladed mixer processes are scaled-up. It is unclear whether a different behavior would be observed as mixer size is scaled-up. We examine the effect of the aforementioned parameters on flow patterns, mixing kinetics, bulk density, granular temperature, particle diffusivity, and pressure and shear-stress profiles. We focus on the effect of these parameters as they pertain to the scale-up of bladed mixer processes, and present some scaling relationships and general guidelines.

Numerical Method

Discrete element method

The discrete element method (DEM) integrates Newton's equations of motion for each particle starting from an initial system configuration. This method provides information regarding the particle's position, velocity and resultant forces. The motion of each particle is described by

$$m_i \frac{dv_i}{dt} = \sum_j (F_{ij}^N + F_{ij}^T) + m_i g \tag{1}$$

$$I_i \frac{d\omega_i}{dt} = \sum_j (R_i \times F_{ij}^T) + \tau_{rij} \tag{2}$$

where m_i, R_i, I_i, v_i and ω_i, respectively, are the mass, radius, moment of inertia, linear velocity, and angular velocity of particle i, and g is the acceleration due to gravity. F_{ij}^N and F_{ij}^T are the normal and tangential forces resulting from the contact of particle i with particle j. The effect of rolling friction is included in the torque term τ_{rij} which is given by $\tau_{rij} = -\mu_r \left| F_{ij}^N \right| R_i \omega_i$. We used the model developed by Tsuji et al.[27] to compute contact forces. This model provides a nonlinear force based on Hertzian contact theory. The normal and tangential forces are given by

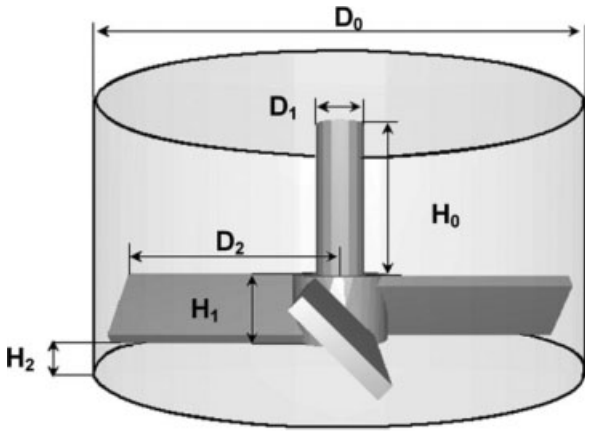

Figure 1. Mixer schematic.

$$F^N = -\tilde{k_n}\delta_n^{3/2} - \tilde{\gamma}_n\dot{\delta}_n\delta_n^{1/4} \tag{3}$$

$$F^T = -\tilde{k_t}\delta_t - \tilde{\gamma}_t\dot{\delta}_t\delta_n^{1/4} \tag{4}$$

where $\tilde{k_n}$ and $\tilde{k_t}$ are the normal and tangential stiffness coefficients, δ_n and δ_t are the normal and tangential displacements, and $\tilde{\gamma}_n$ and $\tilde{\gamma}_t$ are the damping coefficients. The tangential displacement is calculated by

$$\delta_t = \int v_{\text{rel}}^t dt \tag{5}$$

where v_{rel}^t is the relative tangential velocity of the colliding particles, and is defined as

$$v_{\text{rel}}^t = (v_i - v_j)\cdot s + \omega_i R_i + \omega_j R_j \tag{6}$$

In Eq. 6, s is the tangential decomposition of the unit vector connecting the center of the particles. The tangential force is limited by the Coulomb condition $F^T < \mu_s|F^N|$. When the tangential force obtained from Eq. 4 exceeds the Coulomb limit, the tangential displacement is set to $\delta_t = F^T/\tilde{k_t}$ in order to account for slip during a contact. The stiffness coefficients are obtained from

$$\tilde{k_n} = \frac{E\sqrt{2R^*}}{3(1-\sigma^2)} \tag{7}$$

$$\tilde{k_t} = \frac{2\sqrt{2R^*}G}{2-\sigma}\delta_n^{1/2} \tag{8}$$

with E being the particle's Young's modulus, G is the Shear modulus and σ the particle's Poisson ratio. R^* is defined as the effective radius of the contacting particles, and is obtained by

$$R^* = \frac{R_i R_j}{R_i + R_j} \tag{9}$$

The normal damping coefficient is given by

$$\tilde{\gamma}_n = \ln e \frac{\sqrt{m\tilde{k_n}}}{\sqrt{\ln^2 e + \pi^2}} \tag{10}$$

Table 1. Mixer Dimensions

Dimension	Value (mm)
D_0	315
D_1	32.5
D_2	152.5
H_0	245
H_1	45
H_2	10

where e is the coefficient of restitution. In this work, the tangential damping coefficient is assumed to be the same as the normal damping coefficient.

Input parameters and mixer geometry

A schematic of the mixer geometry used in this work is presented in Figure 1. In our coordinate system, the origin is located at the center of the cylinder's bottom plate. Table 1 shows the mixer dimensions that were used for our base case simulations discussed in the sections entitled "The Effect of Fill Level" and "Effect of Particle-Wall Friction". "The effect of varying the H_0 and H_2 dimensions is discussed in the section entitled "The Effect of Blade Position". The section "The Effect of D/d Ratio" outlines the change in granular behavior when the dimensions listed in Table 1 are linearly scaled-up while keeping the particle diameter a constant. The input parameters used for the simulations are listed in Table 2. These values have been shown to afford DEM results comparable to those obtained experimentally with glass beads.[15,17] The physical properties listed in Table 2 were used for the particles, the blades and cylinder walls in all the simulations except the ones discussed in the section entitled "Effect of Particle-Wall Friction". In this section, the sliding friction for the particle-cylinder wall contacts was varied from that of the particle–particle and particle-blade contacts to examine the effect of this parameter on the granular behavior.

The particle bed was composed of monodisperse, cohesionless spheres. Particles are created in the computational space and allowed to settle under gravity, while the blades remain stationary. In the sections entitled "Effect of Particle-Wall Friction" and "The Effect of D/d Ratio", enough particles are created so that the particle-bed height spans the height of the blades. The number of particles created is varied in the sections entitled "The Effect of Fill Level" and "The Effect of Blade Position" to study the effect of mixer fill level. Blade movement is started once particle deposition has been completed. Once the total kinetic energy of the system reaches a constant value, the system is considered to be at steady state and parameter measurements commence. Under

Table 2. Input Parameters

Variable	Symbol	Value
Rolling Friction Coefficient	μ_r	0.005
Sliding Friction Coefficient	μ_s	0.1–0.5
Particle density	ρ_p	2.2 g/ml
Young's modulus	E	2.6×10^6 Pa
Coefficient of restitution	e	0.6
Particle Diameter (d)	d	10 mm
Number of Particles	N	5000–200000
Poisson's ratio	σ	0.25
Time step		$< 1\times10^{-5}$ sec

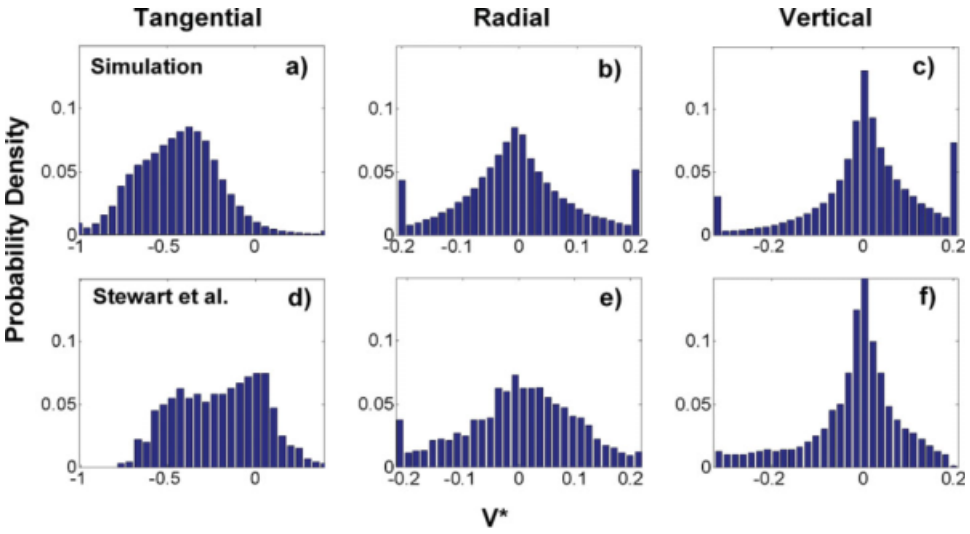

Figure 2. Normalized velocity frequency distributions obtained from simulations vs. experimental results from Stewart et al.[12]

(a)–(c) Simulation frequency distributions for the normalized tangential, radial and vertical velocity components, and (d)–(f) PEPT experimental frequency distributions for the normalized tangential, radial and vertical velocity components. The tangential velocity values shown here are relative to the tip speed of the blades. [Color figure can be viewed in the online issue, which is available at www.interscience.wiley.com.]

these conditions, steady state is reached within 2 s of blade movement. Simulations were performed using blade speeds of 10 and 20 revolutions per minute (RPM). The higher blade speed was used for the simulations discussed in the section entitled "The Effect of D/d Ratio". At these rotational speeds, granular flows in the bladed mixer occur in the quasi-static regime.[14] The blades are rotated counter-clockwise.

Results and Discussion

The effect of fill level

In this section, we describe the fill level inside the mixer by taking the ratio of the particle-bed height prior to blade movement (H) to the mixer diameter (D). H is measured from the bottom plate of the mixer. For the mixer geometry presented in Figure 1, H/D = 0.17 represents an initial particle-bed height covering just the span of the blades. We begin by comparing the particle velocities obtained from our simulations with the experimental results of Stewart et al.[12] obtained using glass beads and positron emission particle tracking (PEPT) in a mixer with two flat blades. Figure 2 shows the velocity frequency distributions for the normalized tangential, radial and vertical velocity components from the simulation with H/D = 0.17 vs. the PEPT experimental results at H/D = 0.12. The velocities presented in Figure 2 have been normalized by the blades' tip speed. The tangential velocities shown are relative to the angular movement of the blades, i.e., $V_t* = (V_t - V_{\text{tip}})/V_{\text{tip}}$. As can be seen from

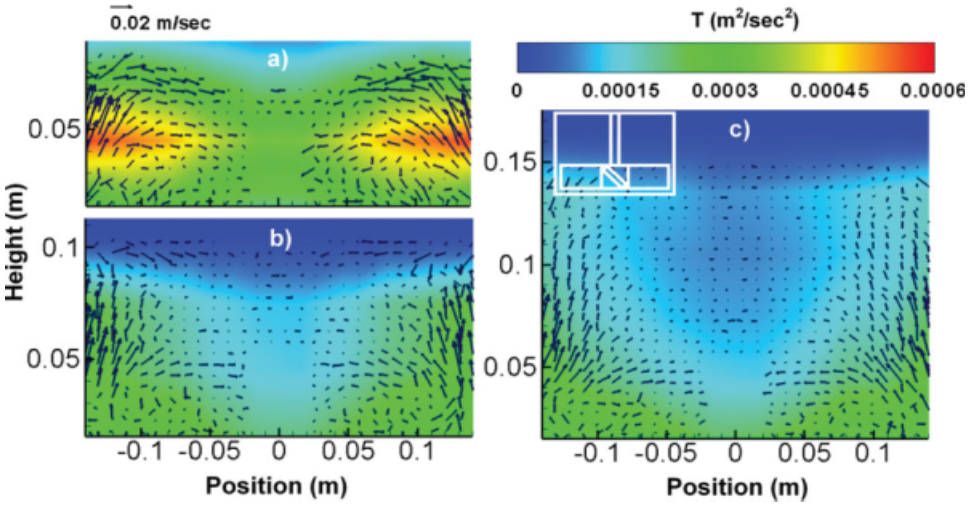

Figure 3. Velocity field in front of blade and granular temperature.

(a) H/D = 0.17, and (b) H/D = 0.32 and c) H/D = 0.46. [Color figure can be viewed in the online issue, which is available at www.interscience.wiley.com.]

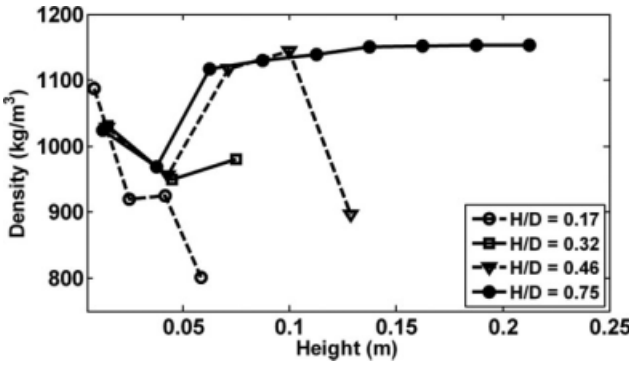

Figure 4. Effect of H/D on bulk density.

Figure 2 the shape of the frequency distributions obtained from the simulation (Figure 2a–c) is very similar to those observed experimentally by Stewart et al. (Figure 2d-f). The tangential velocities in both cases have a left-skewed distribution with most particles having velocities lower than the tip speed of the blades ($V^* < 0$), and a few particle possessing velocities above it ($V^* > 0$). The radial velocities show a normal distribution centered at zero (Figure 2b and 2e), while the vertical velocities have right-skewed distributions (Figure 2c and 2f). For both the simulation case and the experimental case most particles possess radial and vertical velocities which are much lower than the tangential velocities. Some differences are observed between the simulation results and those obtained experimentally. The tails of the radial and vertical velocity distributions are longer than those obtained by Stewart et al. In our simulations we used four blades pitched at an angle and this blade configuration promotes vertical and radial mixing[14] vs. the two flat blades used by Stewart et al. Despite these differences, the general trends are remarkably similar.

A salient feature of granular flows in bladed mixers at fill levels covering just the span of the blades is the formation of heaps where the blades are present and valleys in between blade passes. The formation of these heaps leads to the development of a 3-D recirculation zone in front of the blades which promotes radial and vertical mixing. The development of this recirculation zone leads to enhanced mixing kinetics.[14] This flow structure occurs near the front of the blades, and is not present for the particles in between the blades and behind the blades. In this work, we gauge the effect of the studied parameters on the convective particle motion by examining the flow structures that develop in front of the blades since the development of the recirculation zone is a key flow feature.

We find that, while present at all the fill levels studied, the size and intensity of the recirculation zone in front of the blades is dependent on mixer fill level. Velocity fields in front of the blade and granular temperature contour plots are presented in Figure 3 for different fill levels. The granular temperature is defined as

$$T = \frac{1}{2}\langle u' u' \rangle \tag{11}$$

were u' is the fluctuation velocity, which is the instantaneous deviation from the mean velocity in a control volume around the point being examined. The mean velocity is the averaged velocity for all the particles in the control volume at each time-step. $\langle\rangle$ denotes the temporal averaging of the quantity $u'u'$ within the control volume. The recirculation pattern that forms in front of the blades is most prominent for H/D = 0.17 (Figure 3a). Due to the pitch of the blades, particle rise by the wall forming a heap. The particles on the top of the heap then move radially inward, forcing the particles by the shaft to flow downward and radially outward, leading to the recirculation. The size of the recirculation zone decreases for H/D > 0.17 (Figure 3b and 3c) as heap formation does not occur at these fill levels, and the free surface of the particle bed undergoes almost no deformation. Reduction in the size of recirculation zones as fill level is increased has also been observed experimentally in a mixer with two flat blades.[12] However, the velocity profiles within the span of the blades are very similar for H/D = 0.32 and H/D = 0.46. At H/D > 0.17, a mixing dead zone develops for the particles near the impeller shaft and above the blades. Almost no radial and vertical movement occurs in this zone and particles move mostly in the tangential direction. The size of the mixing dead zone increases with increased fill level. Granular temperature is highest for H/D = 0.17 with temperature maximums occurring at the top tip of the blades. Granular temperature profiles within the span of the blades are similar for H/D = 0.32 and H/D = 0.46. The mixing dead zone observed for H/D > 0.17 coincides with regions of low granular temperature.

Figure 4 shows time-averaged bulk-density profiles as a function of bed height for different fill levels. Lower density values are observed for H/D = 0.17, i.e., the case with the highest granular temperature. At this fill level, bed dilation occurs when the blades rotate due to the development of heaps. Averaged density values increase for H/D > 0.17, since the weight of the particles above the blades hinders heap formation and bed dilation. However, bulk-density values within the span of the blade change little between the H/D > 0.17 cases. This is similar to the behavior observed for the velocity and granular temperature profiles. Thus, for high-fill levels, the portion of the particle bed within the blades' span dilates to a particular density value during flow and this value is independent of fill level. For fill levels significantly higher than the height of the blades (H/D > 0.32), the region above the blades undergoes almost no dilation and density values are close to the averaged bulk density

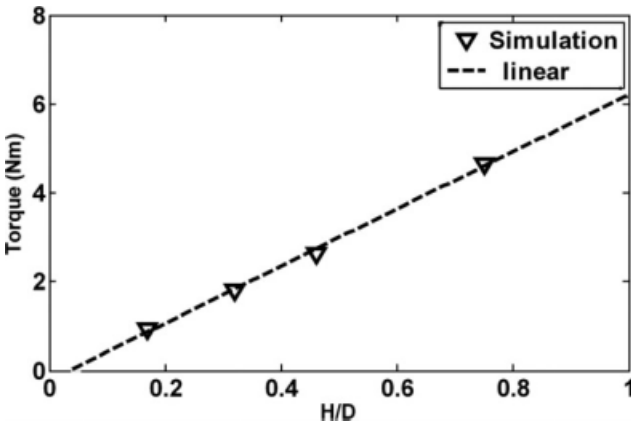

Figure 5. Effect of H/D on impeller torque.

Table 3. Effect of H/D on Particle Diffusivity and Peclet Number for Particles within the Span of the Blades*

H/D	$D_{\theta\theta}$ (m^2/sec)	D_{rr} (m^2/sec)	D_{yy} (m^2/sec)	$Pe_{\theta\theta}$	Pe_{rr}	Pe_{yy}
0.17	4.0×10^{-5}	1.9×10^{-5}	5.4×10^{-5}	360	110	46
0.32	1.3×10^{-5}	7.2×10^{-6}	5.6×10^{-5}	1070	253	48
0.46	1.3×10^{-5}	7.1×10^{-6}	4.4×10^{-5}	1090	260	48

*Particle diffusivities were computed with a Δt of 1/4 of a revolution.

prior to blade movement ($\sim$1200 kg/m^3). While bed dilation within the span of the blades is independent of fill level at H/D $>$ 0.17, the amount of energy needed to induce flow does depend on fill level. Figure 5 shows the average impeller torque as a function of H/D. Impeller torque increases linearly with fill level as the average pressure within the span of the blades increases linearly with particle-bed height. A similar behavior has been observed experimentally for impeller power measurements taken with glass beads at H/D $<$ 2.5.[28] Since impeller torque is independent of rotation rate in the quasi-static regime, our results suggest that a power per unit volume scaling relationship exists in bladed mixers. Therefore, the energy needed to induce flow at high-fill levels could be predicted from torque measurements at lower fill levels.

We gauge particle motion at the microscopic level by calculating particle diffusivities which describe the mass flux rate due to the particles' ''random walk''. The diffusive tensor calculation was taken from Campbell,[29] and is given by

$$D_{ij} = \left\langle (\Delta x_i - \overline{\Delta x_i})(\Delta x_j - \overline{\Delta x_j}) \right\rangle / 2\Delta t \tag{12}$$

where Δx_i represents the particle displacement in the i direction relative to the particle's initial position, $\overline{\Delta x_i}$ is the mean particle displacement, and D_{ij} is the corresponding diffusion coefficient in the i direction due to a gradient in the j direction. Particle diffusivities were computed with a Δt of 1/4 of a revolution, and were averaged over all the particles within the span of the blades. Particle diffusivities were computed in the same manner for the particles located above the blades. The convective and diffusive contributions to particle motion are compared by calculating the Peclet number

$$Pe_{ij} = \frac{U_i R}{D_{ij}} \tag{13}$$

where U_i is the average particle speed in the i direction, R is the mixer radius and D_{ij} is the corresponding diffusion coefficient.

Table 3 lists diffusivity coefficients and Peclet numbers for the particles within the span of the blades at different H/D ratios. Particles diffusivities are the highest for H/D = 0.17 as granular temperature and bed dilation are highest for this case. $D_{\theta\theta}$ and D_{rr} values decrease for H/D $>$ 0.17, but these values change little between the H/D = 0.32, and the H/D = 0.46 cases. The weight of the particles above the blades, which leads to lower granular temperatures and lower degree of bed dilation, hinders particle diffusivity in the radial and tangential direction. However, D_{yy} the value within the span of the blades appears to be independent of fill level. This behavior is explained by the pitch of the blades. When the energy needed to overcome the weight of the particle bed is supplied to the impeller, the 45° angle of the blades pushes material up as the blades rotate. As the particles rise following the convective flow, the frictional interactions add a random component to the particles' motion and diffusion occurs. Thus, D_{yy} the diffusion coefficient changes little with an increase in H/D for particles within the span of the blades. The Peclet numbers obtained for all the fill levels studied are significantly higher than unity indicating that convection is the dominating mechanism for particle transfer. The diffusive process is most significant in the vertical direction Pe_{yy}, as values are lower than $Pe_{\theta\theta}$ and Pe_{rr}. Peclet numbers in the tangential and radial direction are the lowest for the H/D = 0.17 case. This indicates that the diffusive process contributing to particle motion is highest for fill levels just covering the height of the blades. However, Peclet numbers change little between H/D = 0.32 and H/D = 0.46 since bulk-velocity profiles and particle diffusivities change little between these cases. These results are in agreement with the velocity and bulk density trends, and demonstrate that flow kinematics within the span of the blades change little at high-fill levels. The diffusion coefficients observed at H/D $>$ 0.17 for the particles above the blades were 1–2 orders of magnitude lower than the values listed in Table 3.

The results presented thus far show that for H/D $>$ 0.17, two different regions develop in the particle bed, each with different flow characteristics. The first region consists of the particles present within the span of the blades. In this region, dilation occurs and particles can move in the radial and vertical direction due to convective and diffusive motions. The second region consists of the particles above the blades. Here, particles move slowly as a block in the tangential direction and almost no dilation or diffusive movement occurs. These differences in behavior affect the particle mixing patterns obtained in each region. In order to evaluate the degree of mixing obtained for each case studied, particles are colored according to their position prior to blade movement. The cylindrical mixer is sliced in half axially and particles on the left side are colored red, while particles on the right side are colored yellow. The particles have identical properties except their color. We then follow the mixing pattern as blade motion begins. Figure 6 shows some snapshots for the top horizontal view illustrating the mixing patterns obtained at different H/D ratios when the particles on the left and right sides of the impeller are colored differently prior to blade movement. Figure 6a shows snapshots of the mixing patterns obtained at the free surface of the particle bed. Enhanced mixing is obtained for the case of H/D = 0.17 compared to the H/D = 0.32 case. Little mixing is observed at the free surface for the H/D = 0.46 case. After 4.5 revolutions, the H/D = 0.17 system is well mixed and mixing is down to the particle–particle level, while unmixed regions still remain for the H/D = 0.32 and H/D = 0.46. However, enhanced mixing is observed for particles just above the span of the blades at high fill levels (Figure 6b).

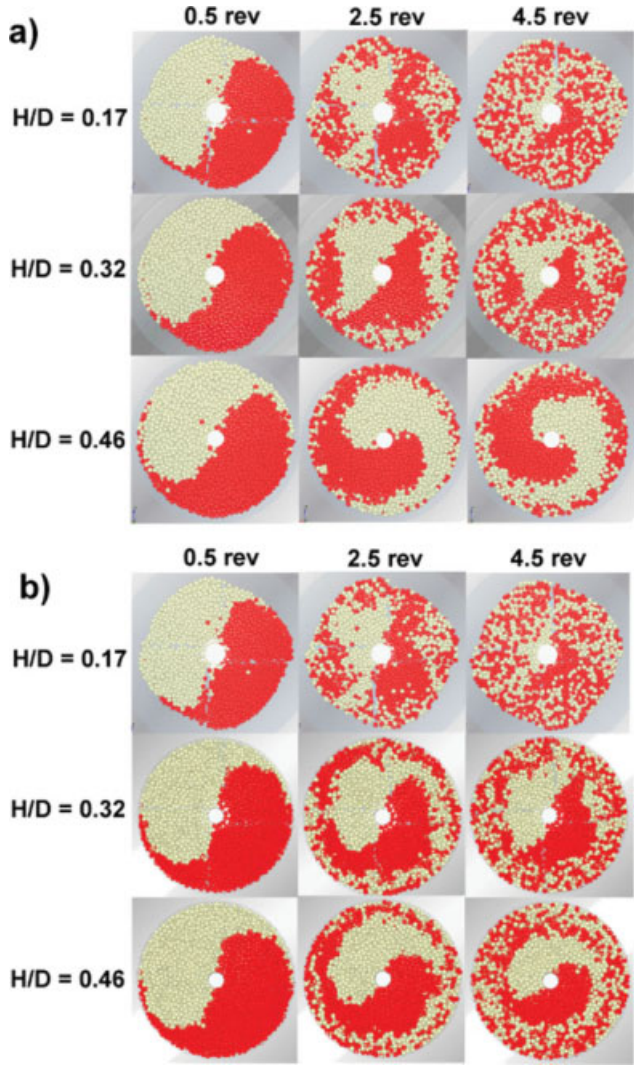

Figure 6. Effect of H/D on mixing.

(a) Snapshot of particles at the free surface, and (b) snapshots of particles above the span of the blades. [Color figure can be viewed in the online issue, which is available at www.interscience.wiley.com.]

Mixing patterns in this region are similar for H/D = 0.32 and H/D = 0.46. This behavior is consistent with particle velocity and diffusivity analysis. Well-mixed zones are first observed by the cylinder wall, the area of highest granular temperature. Thus, the frictional characteristics of the wall facilitate mixing within the span of the blades by increasing the fluctuation velocities. The mixing kinetics of particles by the blades remain the highest for the case of H/D = 0.17 due to the higher particle diffusivities in the tangential and radial direction.

In addition to influencing flow kinematics, fill level affects the stresses that develop inside the mixer during flow. Stress profiles within the granular bed were calculated following the procedure outlined by Campbell.[30] Collisional stresses are obtained from

$$\tau_{ij} = \frac{d}{V_c}\langle F_i k_j \rangle \tag{14}$$

where d is the diameter of the particle, V_c is the control volume, F_i is the total contact force in the i direction, and k_j is the j component of the unit vector connecting the centers of the colliding particles. Stresses in granular systems are known to be scale-dependent.[31] As such, the calculated stress values are affected by the size of the control volume. The control volume size used for the stress tensor calculation was determined by varying this parameter until the values obtained were independent of control volume size (~5 particle diameters). The collisional stress tensor was calculated in a 3-D cylindrical coordinate system. Our analysis showed that a symmetric stress tensor is obtained following this procedure (i.e., $\tau_{\theta r} = \tau_{r\theta}$). In this work, only the contribution of collisional stresses is considered as kinetic stresses were found to be three-orders of magnitude smaller. Since the rotational motion of the blades determines the main shearing direction, we focused our attention on the average normal stress and the shear-stress component in the plane of the blade rotation $\tau_{\theta r}$. From the normal stresses, the pressure inside the particle bed is given by

$$P = \frac{1}{3}\left(\tau_{\theta\theta} + \tau_{rr} + \tau_{yy}\right) \tag{15}$$

where $\tau_{\theta\theta}$, τ_{rr}, and τ_{yy} are the normal stresses in the tangential, radial and vertical direction, respectively.

Figure 7 shows time-averaged pressure profiles as a function of height at different H/D ratios. We find that for H/D = 0.17 and H/D = 0.32, the temporal-averaged pressure inside the mixer can be approximated by the simple hydrostatic pressure relationship $P = \rho_{\text{bulk}} g(h - H_{\text{bed}})$. In this formula ρ_{bulk} is the overall time-averaged bulk density of the granular bed (determined from Figure 4), g is the acceleration due to gravity, h is the vertical position and H_{bed} is the total height of the particle bed. However, when the H/D ratio is above 0.46, two distinct regions develop in the pressure profile. The first region consists of a hydrostatic regime where the pressure is proportional to the height of the bed. The second region consists of a saturated regime where pressure is independent of bed height. The development of a saturated region in static systems is predicted by the classical Janssen equation.[32] However, in our system the height at which the saturated regime begins is the same for H/D =

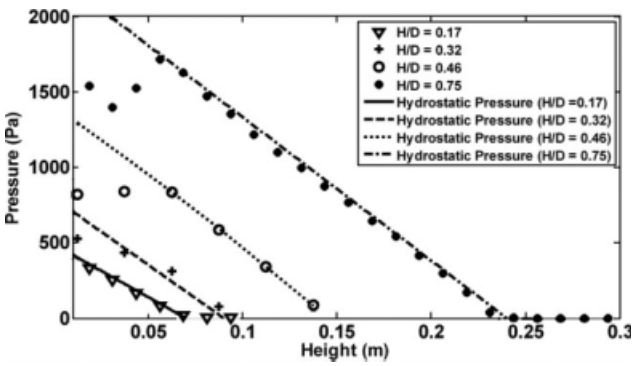

Figure 7. Time-averaged pressure for particles within the mixer vs. height.

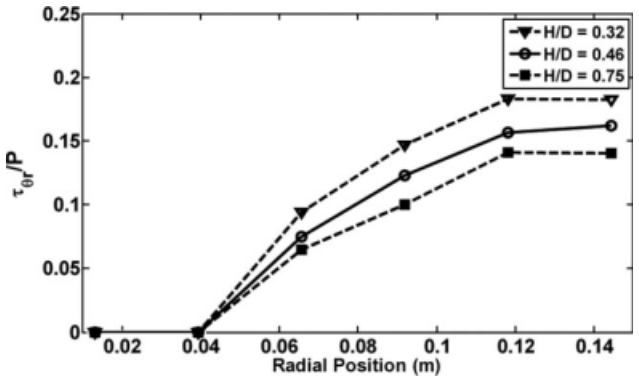

Figure 8. Time-averaged bulk friction for particles within span of blade vs. height.

0.46 and H/D = 0.75 and coincides with the height of the 3-D recirculation zone present in front of the blade. This is different from what the Janssen equation predicts. In static systems, the saturated regime begins at a height where the hydrostatic pressure is equal to a critical pressure value. At this height, normal stresses are transferred to the cylinder walls via stable contact chains, and the walls begin to support the weight of the particle bed. The critical pressure value is a function of the particle-wall angle of internal friction and the cylinder's diameter.[33,34] Thus, in static systems, the span of the saturated regime increases with total bed height. However, in our bladed mixer, the span of the saturated regime does not change when the total bed height is increased and it is independent of pressure. This suggests that the cylinder walls in the bladed mixers we have examined do not bear the load of the particle-bed weight.

The saturated pressure regime observed for H/D > 0.46 develops as a result of two contributing factors; the decrease in bed dilation and the 45° angle of the blades. Since the expansion of the particle bed during flow is limited by the weight of the particles above the blades, the load associated with the weight of the particles within the span of the blade is transferred to the impeller. The pitched angle of the blades allows the impeller to support the weight of these particles leading to the almost constant pressure region. The linear relationship obtained between impeller torque and fill level (Figure 5) confirms that the particle-bed weight is being carried by the impeller and not the cylinder walls. If the weight of the particle bed were supported by the cylinder wall at high H/D, the torque experienced by the impeller for the H/D = 0.46 case would the same as for the H/D = 0.75 case. The increase in impeller torque indicates that this is not case. Additionally, the Janssen equation predicts that much higher bed heights are needed for the saturated regime to be encountered for the frictional properties of our system. This behavior, while analogous to the Janssen effect in that a constant pressure is observed, is a result of the blade configuration and not the transfer of normal stress to the walls via stable contact chains.

Figure 8 shows the time-averaged shear stress to pressure ratio $\tau_{\theta r}/P$, also known as the bulk friction coefficient, for the particles within the span of the blade at different fill levels. As can be seen from Figure 8, the bulk-friction coefficient is higher for the particle closes to the wall. As the averaged pressure remains constant in the radial direction,[14]

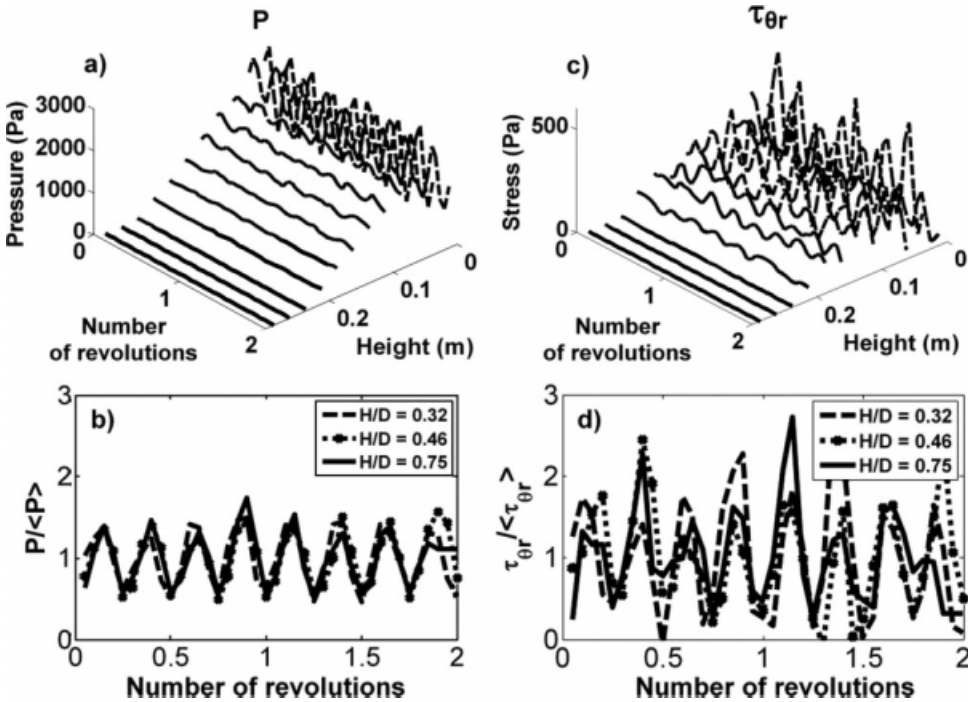

Figure 9. Pressure and shear-stress fluctuations at r = 0.09 m.

(a) Pressure fluctuations as a function of height and number of revolutions for H/D = 0.75, (b) Normalized pressure fluctuations for particles within span of blade, (c) $\tau_{\theta r}$ fluctuations as a function of height and number of revolutions for H/D = 0.75, and (d) Normalized $\tau_{\theta r}$ fluctuation for particles within span of blade.

the increase in bulk friction is due to an increase in shear stress. Increased shear stress near the mixer walls has been observed experimentally by Watano et al.[35] in a high-shear mixer. Figure 8 also shows that the $\tau_{\theta r}/P$ ratio decreases as H/D increases. The bulk friction is the highest for case where a hydrostatic pressure relationship is obtained within the span of the blades (H/D = 0.32). Bulk friction decreases for the cases where the pressure within the span of the blades is independent of height. The amount of momentum transferred in the shearing direction relative to the compression state of the system decreases when the impeller supports the weight of the particle bed. However, the decrease in the ratio is ~22% between the values obtained for H/D = 0.32 and H/D = 0.75. This is a relatively small decrease when we consider that the average pressure increases by a factor of 3 between these two cases.

Figure 9 shows the temporal pressure and shear-stress profiles that develop during flow at a radial position of $r = 0.09$ m. The pressure profile obtained for the H/D = 0.75 case is presented in Figure 9a as a function of height and number of revolutions. Periodic pressure fluctuations develop within the span of the blades with a main fluctuation frequency equal to the blade rotation. These pressure fluctuations exist in the saturated pressure regime region. Thus, the mean and amplitude of the pressure fluctuations are constant in this region. No fluctuations are observed for the region above the span of the blades. This is slightly different from the behavior observed for the bladed mixer flows for H/D = 0.17, where the pressure fluctuations are present throughout the span of the particle bed.[14] In Figure 9b, we compare the normalized pressure fluctuations obtained within the span of the blades at different H/D ratios at a radial position of $r = 0.09$ m. The normalized pressure is obtained by dividing the instantaneous pressure by the temporal averaged pressure at this position $\langle P \rangle$. Figure 9b shows that the pressure fluctuates between 0.5 $\langle P \rangle$ and 1.5 $\langle P \rangle$ regardless of fill level. This suggests that the resulting pressure fluctuations within the span of the blades can be scaled according to fill level. If the average pressure is known, then the pressure fluctuations can be predicted. As shown in Figure 7, the average pressure can be determined from hydrostatics for low-fill levels. For high-fill levels, the average pressure within the span of the blades can be approximated by the hydrostatic pressure right above the blades.

Figure 9c shows the $\tau_{\theta r}$ fluctuations as a function of height and number of revolutions for H/D = 0.75. The shear-stress profile shows a periodic behavior similar to the one observed for pressure. The mean and amplitude of the $\tau_{\theta r}$ fluctuations are relatively constant within the span of the blades. While $\tau_{\theta r}$ fluctuations are observed above the span of the blades, the mean and amplitude of these fluctuations decrease toward the top of the particle bed. Figure 9d presents the normalized $\tau_{\theta r}$ fluctuations at different H/D ratios. Although the normalized $\tau_{\theta r}$ profiles show some scatter which was not observed in the pressure profiles, the maximum and minimum fluctuation values are similar for all the H/D ratios. $\tau_{\theta r}$ fluctuates between a minimum value of zero and a maximum value of ~3 $\langle \tau_{\theta r} \rangle$. Since pressure profiles can be approximated by hydrostatics, our results suggest that if the value of the bulk-friction coefficient inside the particle bed is known, then the $\tau_{\theta r}$ profiles could also be approximated from hydrostatics. Similar to pressure, the resulting fluctuations can be scaled according to fill

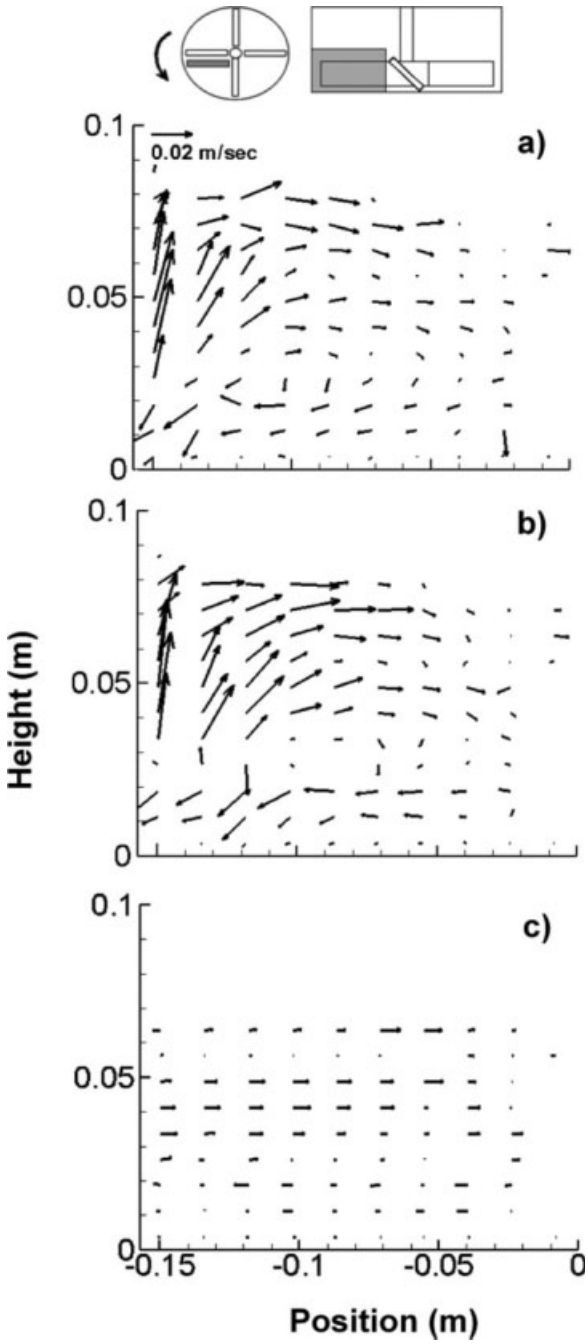

Figure 10. Effect of particle-wall and particle–particle friction on velocity field in front of blade.

(a) $\mu_s^{p-p} = \mu_s^{p-w} = 0.5$, (b) $\mu_s^{p-p} = 0.1$, $\mu_s^{p-w} = 0.5$, and (c) $\mu_s^{p-p} = 0.5$, $\mu_s^{p-w} = 0.1$.

level. The trends reported in this section are applicable to monodisperse, cohesionless spheres in the quasi-static regime. A more comprehensive study is needed exploring the effect of polydispersity, particle shape and interparticle cohesion on the results presented here.

Effect of particle-wall friction

As mentioned earlier, the development of a 3-D recirculation zone in front of the blades is a key flow feature in

Table 4. Effect of Particle-Wall and Particle-Particle Friction on Particle Diffusivity and Peclet Numbers*

μ^{p-p}	μ^{p-w}	$D_{\theta\theta}$ (m^2/sec)	D_{rr} (m^2/sec)	D_{yy} (m^2/sec)	$Pe_{\theta\theta}$	Pe_{rr}	Pe_{yy}
0.5	0.5	4.0×10^{-5}	1.9×10^{-5}	5.4×10^{-5}	360	110	46
0.1	0.5	1.7×10^{-5}	7.5×10^{-6}	1.7×10^{-5}	900	217	117
0.5	0.1	4.6×10^{-8}	1.9×10^{-8}	2.3×10^{-8}	>300000	>10000	>5000

*Particle diffusivities were computed with a Δt of 1/4 of a revolution and were averaged over all the particles in the computational domain.

bladed mixers. As such, developing an understanding of the parameters leading to the formation of this flow pattern is critical for the design and operation of bladed mixers. In this section, the total height of the particle bed just covers the span of the blades (i.e., a fill level of H/D = 0.17). The influence of the particle-boundary frictional characteristics when they differ from those of the particle–particle interaction was examined. We find that the development of the 3-D recirculation pattern is strongly dependent on the particle-cylinder wall sliding friction coefficient. Figure 10 shows the time-averaged velocity fields in front of the blade in the vertical plane for different combinations of particle–particle sliding friction (μ_s^{p-p}), and particle-cylinder wall sliding friction (μ_s^{p-w}). Heap and vortex formation occurs when wall friction is high (0.5) as can be seen from Figure 10a and b. Particles rise by the wall forming a heap as the impeller is moved. The formation of these heaps leads to the development of the recirculation zone. Lowering particle friction from 0.5 to 0.1 for high-wall friction had a small effect on the velocity profile in front of the blade (Figure 10b). However, at high-particle friction (0.5), and low-wall friction (0.1), no heap or vortex formation occurs (Figure 10c). The absence of the heap leads to low radial and vertical velocities, and the recirculation zone cannot develop. Particles move as a block solely in the tangential direction. Changing the particle-blade sliding friction coefficient had a negligible effect on the resulting velocity profiles.

We have postulated in the past that the formation of these heaps is due to the development of contact force chains when the granular bed is compressed in front of the blade.[14] A force chain is a network of interparticle contacts in which force is transmitted along the contact path. The formation of stable contact chains has been demonstrated to be a function of wall friction in dynamic systems such as discharging silos.[36] At low-particle-wall friction, stable contact force chains do not form, particles slide past the wall as they get pushed by the blade and cannot rise; thus, the heap and the recirculation zone cannot develop. Slippage of the particles near the wall is decreased as wall friction is increased. For high-wall friction values, we find that a particle layer two particle diameters in length forms at the wall, which has an average velocity of 50–60% of the blades' tip speed. The reduced particle velocities are due to the stick-slip motion that occurs by the wall. This stick-slip behavior allows the formation of stable contact chains that lead to heap formation and, consequently, the 3-D recirculation. However, at low-wall friction values, the particles in contact with the wall flow at a velocity equal to the blade tip speed. A significant amount of friction at the cylinder wall appears to be necessary in bladed mixers to induce radial and axial flow.

Table 4 shows the particle diffusivity in the tangential direction ($D_{\theta\theta}$), the radial direction (D_{rr}) and the vertical direction (D_{yy}) at different values of wall friction and particle friction. Particle diffusivities are highest for the case of high-wall friction and high-particle friction. We have shown in our previous work that frictional contacts in bladed mixers lead to an increase in fluctuating kinetic energy,[14] which is indicative of an increase in the random motion of the particles. When frictional collisions occur, the resulting particle velocities differ from that of the bulk flow. This effect increases with higher friction coefficients leading to higher particle diffusivities. When particle friction is decreased from 0.5 to 0.1 at high-wall friction, diffusivity values decrease to about 40% of the observed values at $\mu_s^{p-p} = 0.5$. However, when wall friction is decreased to 0.1 at high-particle friction, particle diffusivities drop by 2–3 orders of magnitude. These results show that the frictional cylinder walls act as the main source of fluctuating kinetic energy in the bladed mixer. Similar trends were observed for the cross diagonal terms of the diffusive stress tensor.

Table 4 also shows values for the Peclet number in the tangential, radial and vertical direction. The lowest Peclet numbers are obtained for the case of high-wall friction and high-particle friction. The diffusional contribution to particle transport is the highest for the most frictional system. Peclet numbers increase for the case of high-wall friction and low-particle friction. As can be seen from Figure 10b, the convective flow profile remains unaffected by the decrease in particle friction while particle diffusivities are reduced. At high-wall friction and low-particle friction, the diffusive process all but shuts down. For this case, particles essentially move along the tangential direction in streamlines which the particles do not cross nor diffuse in and out of.

The effect of the convective and diffusive processes on mixing kinetics can be quantified by computing the relative

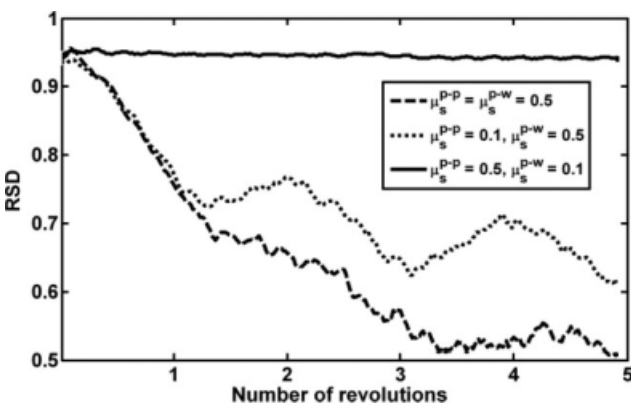

Figure 11. Effect of particle-wall and particle–particle friction on mixing.

Relative standard deviation of red particle concentrations vs. number of revolutions.

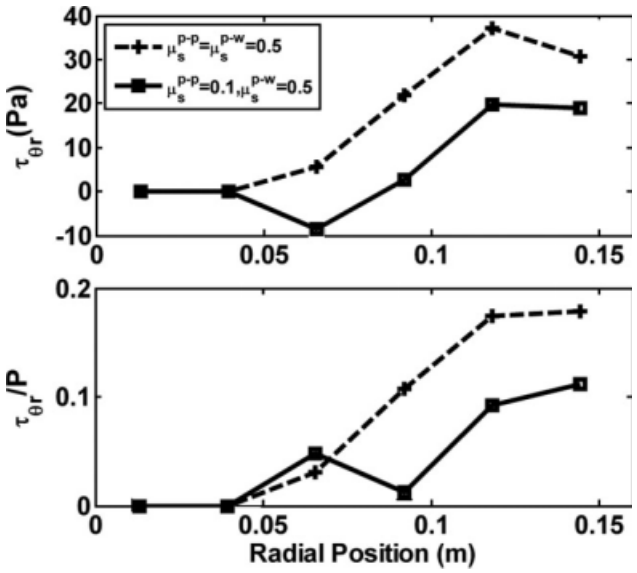

Figure 12. Effect of particle-wall and particle–particle friction on the time-averaged shear stress and bulk-friction coefficient.

(a) $\tau_{\theta r}$ and (b) $\tau_{\theta r}$/P.

standard deviation (RSD) of the red particle concentration for the entire system. As mentioned in the section entitled ''The Effect of Fill Level'', prior to blade movement the mixer is split in half along the axis of the impeller, and the particles on the left side are colored yellow, while the particles on the right are colored red. The RSD is obtained from the following formula

$$\mathrm{RSD} = \frac{\sigma_{\mathrm{conc}}}{M_{\mathrm{conc}}} \tag{16}$$

where σ_{conc} is the standard deviation of the red particle concentration over all the samples taken, and M_{conc} is the overall mean concentration of red particles. The RSD value obtained can be highly sensitive to sample size and sample number. The sample grid size for the RSD calculation was determined by varying the sample number and size until the RSD value obtained was independent of sampling grid. RSD curves for the different wall and particle friction cases are shown in Figure 11. Enhanced mixing is observed for high values of wall friction. No mixing occurs at $\mu_s^{p-p} = 0.5$ and $\mu_s^{p-w} = 0.1$. After roughly three revolutions the RSD curves for the high-wall friction cases begin to level off indicating that the mixing process is down to the particle level. On the other hand, RSD values remain at 0.9 for the low-wall friction case. This behavior is explained by the absence of the 3-D recirculation zone at these frictional conditions. The presence of this vortex promotes convective mixing. However, in addition to convective mixing, diffusive mixing appears to play an important role in this system. While little difference is observed in the velocity patterns for the two cases of high-wall friction (Figure 10a and 10b), the RSD trends show a difference in mixing performance. The enhanced mixing kinetics observed for the higher particle friction case is explained by the higher particle diffusivities which promote diffusive mixing. While convective mixing is the dominant process in this system, diffusive mixing becomes important when the homogenization process is down to the particle–particle level.

Time-averaged values for the $\tau_{\theta r}$ shear stress are shown in Figure 12 for the cases of high-wall friction. As can be seen from Figure 12a, $\tau_{\theta r}$ is the highest for the most frictional system ($\mu_s^{p-w} = \mu_s^{p-p} = 0.5$). Decreasing to 0.1 reduces $\tau_{\theta r}$ by roughly 50%. The values of $\tau_{\theta r}$ are highest near the cylinder wall in both cases and close to zero near the impeller shaft (Figure 12a). Increased shearing by the wall is a byproduct of the stable force chains that form due to wall friction. $\tau_{\theta r}$ values for the case of high μ_s^{p-p} (0.5), and low μ_s^{p-w} (0.1) lie between the two curves shown in Figure 12a. Shear stresses are strong functions of friction, since granular flows in bladed mixer occur in the quasi-static regime at low-rotational speeds like the one used here. While momentum transfer is affected by the frictional characteristics of the cylinder wall, shear stresses inside the particle bed are most sensitive to changes in μ_s^{p-p}. Figure 12b shows the time-averaged bulk-friction coefficient $\tau_{\theta r}/P$. We can see that the $\tau_{\theta r}/P$ ratio is a function of radial position and the system's frictional characteristics. This ratio is highest for the case of high-wall friction and particle friction since pressure profiles are unaffected by changes in particle friction. The values obtained for $\tau_{\theta r}/P$ are much lower than the maximum sliding friction coefficient in the system (0.5). Bulk-friction coefficients lower than the microscopic sliding friction coefficient has also been observed in quasi-static shear flows.[30] This implies that while momentum transfer is affected by friction at the microscopic level, the conditions at which the granular bed deforms are different from what is predicted by Coulomb's law for the particle–particle and particle-wall interactions.

The effect of blade position

In some industrial bladed mixer processes, such as in filter dryers, it is common to change the position of the blade when processing at high-fill levels to enhance mixing and heat transfer. We now look at the effect of changing the position of the blades along the vertical axis at a fill level of H/D = 0.75. Simulations were performed for three different gap heights between the bottom of the blades and the bottom plate: a 10 mm gap (bottom blade position), a 110 mm gap (middle blade position), and 180 mm gap (top blade position). The apparent fill levels relative to the bottom of the blades are H/D = 0.22 for the top blade position, H/D = 0.44 for the middle, and H/D = 0.75 for the bottom. Figure 13a through 13c show the velocity fields and granular-temperature profiles obtained in front of the blade at the different blade position. For the top blade position, a strong recirculation zone develops where the blades are present (Figure 13a). Vertical and radial velocities are high and free surface of the bed deforms by forming heaps. High-granular temperatures are achieved in this area. This behavior is analogous to what was obtained for the H/D = 0.17 case at the bottom blade position. However, the granular temperature obtained within the span of the blades is higher for the top blade position when compared to the H/D = 0.17 case. When the blades are in the top position, the particles just below the blades act as a rough bottom plate. In the previous section we demonstrated that increasing wall friction leads to a

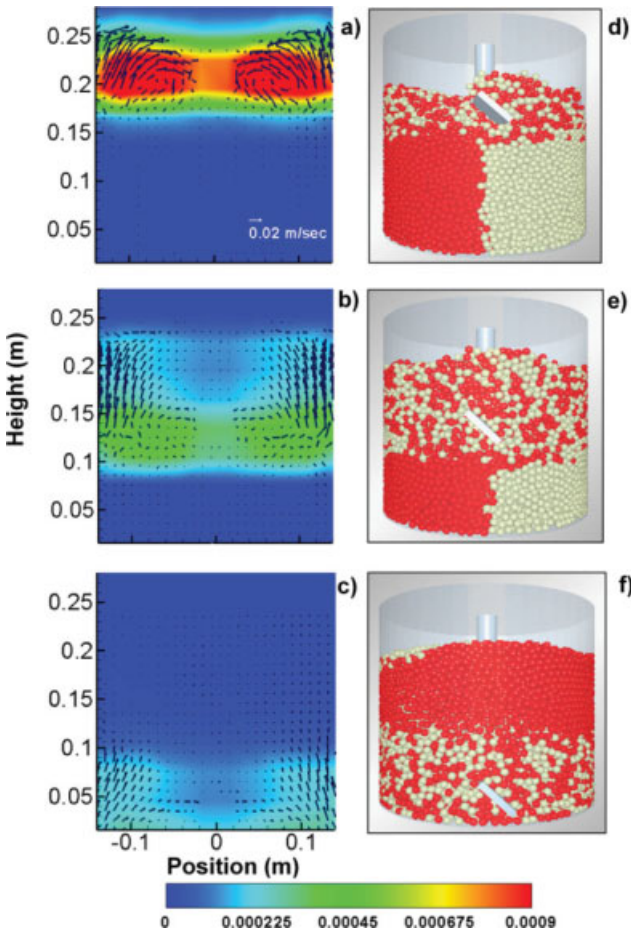

Figure 13. Effect of blade position on velocity fields, granular temperature and mixing patterns at H/D = 0.75.

(a)–(c) Velocity fields in front of blade and granular temperature for different blade positions, and (d)–(f) side view snapshot of mixing after five revolutions. [Color figure can be viewed in the online issue, which is available at www.interscience.wiley.com.]

higher fluctuating kinetic energy of the particles. We hypothesize that this "rough surface," which is not present when the blades are in the bottom position, causes the increase in granular temperature. The region below the blades in Figure 13a is characterized by almost no particle movement and granular temperatures close to zero.

The size of the recirculation zone decreases when the blades are in the middle position (Figure 13b). The weight of the particle above the blades hinders heap formation decreasing the intensity of the recirculation zone. Granular temperature within the span of the blades is lower than for the top blade position case since the load from the particles on the top reduces bed dilation. These characteristics parallel the behavior observed for the H/D $>$ 0.17 cases at the bottom blade position. The only difference between the H/D $>$ 0.17 cases and the middle blade position case is the higher granular temperature within the span of the blade obtained in the latter. This is due to the "rough surface" formed by the particles just below the blade at the middle position. As in the top-blade-position case, the particles beneath the blades remain stationary as the blades rotate. When the blades are positioned at the bottom, the size of the recirculation zone decreases even further along with the granular temperature (Figure 13c). However, the granular temperature within the span of the blades in this case is the same as in the other H/D $>$ 0.17 cases with the blades on the bottom. This confirms that the increase in granular temperature observed for the top and middle blade positions was due to the "rough surface" formed by the particles below the blades.

Figure 13d through 13f show side view snapshots after five revolutions demonstrating mixing patterns achieved for the different blade positions. Two zones developed in all the cases studied, a well-mixed zone and an unmixed region. For the top blade position, a well-mixed region exists within the span of the blades which coincides with the region where the recirculation zone develops (Figure 13d). No mixing occurred below the blades. The majority of the particle bed remains unmixed when the blades are located at the top. When the blades are positioned in the middle, the size of the well-mixed zone increases as it includes the particles located within the span of the blades, as well as those above the blades (Figure 13e). No mixing occurs in the region below the blades. With this blade configuration, a little less than 50% of the particle bed remains unmixed. For the bottom blade position case (Figure 13f), the height of the well-mixed zone is $\sim$100 mm. No particle mixing occurs above this height, which represents roughly 50% of the particle bed. Based on these results, an efficient strategy to improve mixing in bladed mixers at high-fill levels is to alternate between the bottom, and the middle blade positions during processing. By doing this, the portions of the particle bed where particle velocities are low at these two blade positions get agitated and subsequently mixed. Placing the blades toward the top of the particle bed is very inefficient in terms of mixing, since a large portion of the particle bed remains unmixed.

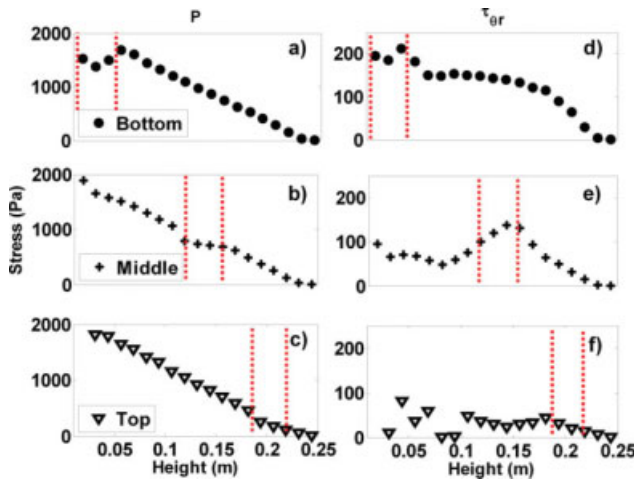

Figure 14. Time-averaged pressure and sheer-stress profiles for different blade positions for H/D = 0.75.

(a)–(c) pressure profiles as a function mixer height, and (d)–(f) $\tau_{\theta r}$ profiles as a function of mixer height. The position of the blades is given by dashed lines in each graph. [Color figure can be viewed in the online issue, which is available at www.interscience.wiley.com.]

The time-averaged pressure and shear-stress profiles are presented in Figure 14 for the different blade positions for a fill level of H/D = 0.75. As was seen earlier, for the bottom blade position, the pressure within the span of the blades is independent of height, while a hydrostatic region exists above the blade (Figure 14a). A similar behavior is observed for the middle blade position. The pressure above and below the span of the blades follows a hydrostatic relationship while it is height independent where the blades are present (Figure 14b). This is not a surprising behavior, since the height of the particle bed above the blades is equivalent to an H/D = 0.44 case for a bottom blade position. The linear pressure profile observed below the span of the blades supports the conclusion that the weight of the particle bed in the saturated regime is supported by the impeller and not the cylinder wall. Two hydrostatic regions develop for the top blade position; one region below the blades with an average bulk density of $\sim$1000 kg/m^3, and a second within the span of the blades with a bulk density of $\sim$800 kg/m^3 (Figure 14c).

The $\tau_{\theta r}$ profile for the bottom blade position case is shown in Figure 14d. Shear stress is highest in the region spanning the blades. $\tau_{\theta r}$ is also fairly constant in this region. Above the blades shear stress is reduced and two regions can be distinguished, one region with a constant shear stress, and another with a more or less linear relationship. The constant shear-stress region develops as stresses get transferred via contact chains from the region within the blades. The linear region begins at the height where the contact chains end. The shear stress in this region follows the pressure trend. For the middle blade position, increases $\tau_{\theta r}$ linearly within the span of the blades and reaches a maximum at the top of the blades (Figure 14e). Below the blades, a fairly constant $\tau_{\theta r}$ region develops due to the transfer of stress via contact chains that originate within the span of the blades. Above the span of the blades, $\tau_{\theta r}$ decreases in a similar way to what is obtained for the bottom blade position in this region. The lowest values of $\tau_{\theta r}$ are achieved with the top blade configuration (Figure 14f). Here, shear stress is constant within the span of the blades and decreases linearly above the blades. Below the blades, a constant shear-stress region develops as observed for the middle blade position. A third region arises toward the bottom plate. In this region, the shear stress exhibits large fluctuations with points of zero shear stress observed. The contact chains that originate within the span of the blades are not long enough to reach the region near the bottom plate. The randomness of the shear stress in this region is consistent with the stress profiles found in static piles, where stresses follow a random path depending on where particle contacts occur.[33]

The effect of D/d ratio

The ratio of mixer diameter to particle diameter (D/d) has been shown to be an important parameter in other granular processes, and it is one of the parameters that changes during scale-up. In this section, we study the effect of varying mixer diameter, while keeping a constant particle diameter. We compare the granular behavior observed in bladed mixers at D/d ratios of 31.5, 63.0 and 94.5. For the parameters used in this work, the range of D/d ratios studied includes mixer sizes ranging from 10 L to 300 L. The mixer dimensions for the D/d = 31.5 case are the ones listed in Table 1. The dimensions of the D/d = 63.0 system are a 2× linear scale-up of the values shown in Table 1. The D/d = 94.5 dimensions are three times the Table 1 values. The only dimension that is kept constant for all mixer sizes is H_2, the gap between the bottom plate and the bottom of the blades. The rotational speed of the blades was set at 20 RPM for all the mixer sizes. The fill level was set to H/D = 0.17 for all the D/d cases studied. In order to compare the results obtained at the different system sizes, and to allow for plotting in the same axis, we normalized all particle velocities relative to the tip speed of the blades V_{tip}. Particle positions are normalized by the total bed height (H) in the vertical direction and by the mixer radius (R) in the radial direction.

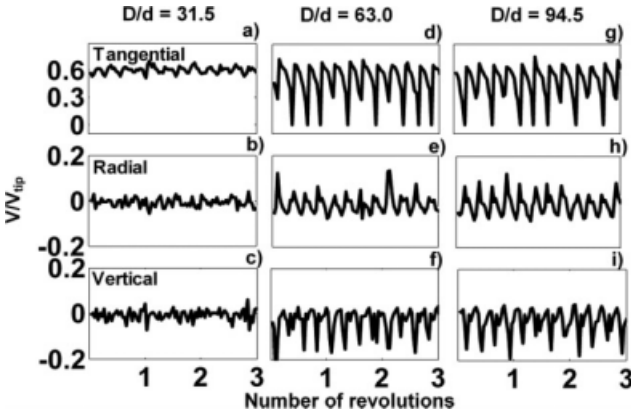

Figure 15. Velocity profiles at r/R = 0.57, y/H = 0.60.

(a)–(c) for D/d = 31.5, (d)–(f) for D/d = 63.0, and (g)–(i) for D/d = 94.5.

Normalized instantaneous velocity profiles at radial position r/R = 0.57 and height y/H = 0.6 are shown in Figure 15 for the different D/d ratios. A cubic control volume with dimensions of $6d \times 6d \times 6d$ was created at these coordinates. The velocity components were calculated by averaging over the control volume at a particular time-step. Since the control volume size was kept constant for all D/d ratios, the velocity values shown in Figure 15 were obtained by averaging over the same number of particles. Tangential velocity fluctuations are observed for all the D/d ratios (Figure 15a, d and g). These fluctuations develop since the particles in front of the blade have a higher tangential velocity than the particles behind the blades.[14] The main frequency of the fluctuations is equal to the rotation frequency of the blades for each D/d case. While the fluctuation period is the same for all the D/d ratios, a difference is observed in the amplitude of the fluctuations. The amplitude of the tangential velocity fluctuation is the lowest for the D/d = 31.5 case, while higher amplitudes are obtained for the D/d = 63.0 and D/d = 94.5 cases. Little difference is seen between the tangential velocity curve for D/d = 63.0, and that for D/d = 94.5. The higher fluctuation amplitudes suggest that particle movement in the tangential direction is less uniform for D/d > 31.5.

Radial and vertical velocity profiles are shown in Figure 15b through 15i for each of the D/d cases. Both the radial and vertical velocity components fluctuate around zero and

are much lower than the corresponding tangential velocity for all the D/d ratios. Periodic fluctuations of higher amplitudes are obtained at D/d = 63.0 and D/d = 94.5 for the radial (Figure 15e and h) and the vertical (Figure 15f and i) velocities. As with the tangential velocity, the curves obtained at D/d = 63.0 are very similar to the ones obtained at D/d = 94.5. The radial and vertical velocities at D/d = 31.5 show less of a periodic behavior and the fluctuation amplitude is much lower compared to the higher D/d ratios. The differences in radial and vertical velocities observed at D/d = 31.5 can be explained by the height of the heaps that develop in front of the blades. While heaps form at every D/d value, the total height of the heaps increases at the higher D/d ratios. The higher heap heights lead to an increase in the potential energy of the particles. This potential energy is then transferred into kinetic energy in the vertical and radial directions as particles flow in and out of the heaps at the larger D/d ratios.

Figure 16 depicts time-averaged radial and vertical velocity fields for the particles in front of the blades in the vertical plane at the different D/d values. The magnitude of the tangential velocity is represented by the color of the vectors. The flow pattern obtained in front of the blade is independent of the D/d ratio as the recirculation zone is present in all the D/d values studied. However, the recirculation zone is most prominent for D/d = 63.0 and D/d = 94.5 (Figure 16a and b). Lower radial and vertical velocities are observed near the bottom plate, cylinder walls, and at the top of the heap for the D/d = 31.5 case (Figure 16c). The lower velocities near the boundaries are due to the effect of wall friction, which is stronger at the low D/d ratio. Boundary friction effects have been previously shown to be scale-dependent on dense granular flows.[37] The lower velocities at the top of the heap are a result of the reduced potential energy at D/d = 31.5, as previously explained. These results suggest that, if the system size is big enough so that the effects of wall friction are minimized, the convective particle motion is independent of system size and can be scaled by the rotational speed of the blades.

Particle diffusion has been previously shown to be dependent on system geometry and size in dense granular flows.[38] Table 5 presents the normalized diffusion coefficients in the tangential, radial and vertical direction obtained for the different D/d ratios. Particle diffusivities were normalized by the tip speed of the blades and the mixer diameter, i.e., $D^*_{\theta\theta} = {}^{D_{\theta\theta}}/_{DV_{tip}}$. Lower normalized particle diffusivities are obtained for the D/d = 31.5 in the tangential, radial and vertical direction, while higher values were observed at D/d = 63.0 and D/d = 94.5. The normalized diffusion coefficients values change little for D/d > 31.5, similar to the behavior observed for the convective particle motion. Therefore, above a certain system size (D/d ≥ 63.0 in our case), particle diffusivity scales linearly with mixer diameter and blade speed. Peclet numbers (see Eq. 13) for the different D/d ratios are also shown in Table 5. All the Peclet numbers obtained are much higher than unity indicating that convection is the main mechanism for particle motion regardless of system size. While convection dominates the transport process, the diffusive contributions increase for the D/d = 63.0 and D/d = 94.5 cases as Peclet numbers decrease roughly by ½ from those observed at D/d = 31.5. The increase in particle diffusivity can be explained by the increase in velocity fluctuations observed at the higher D/d values.

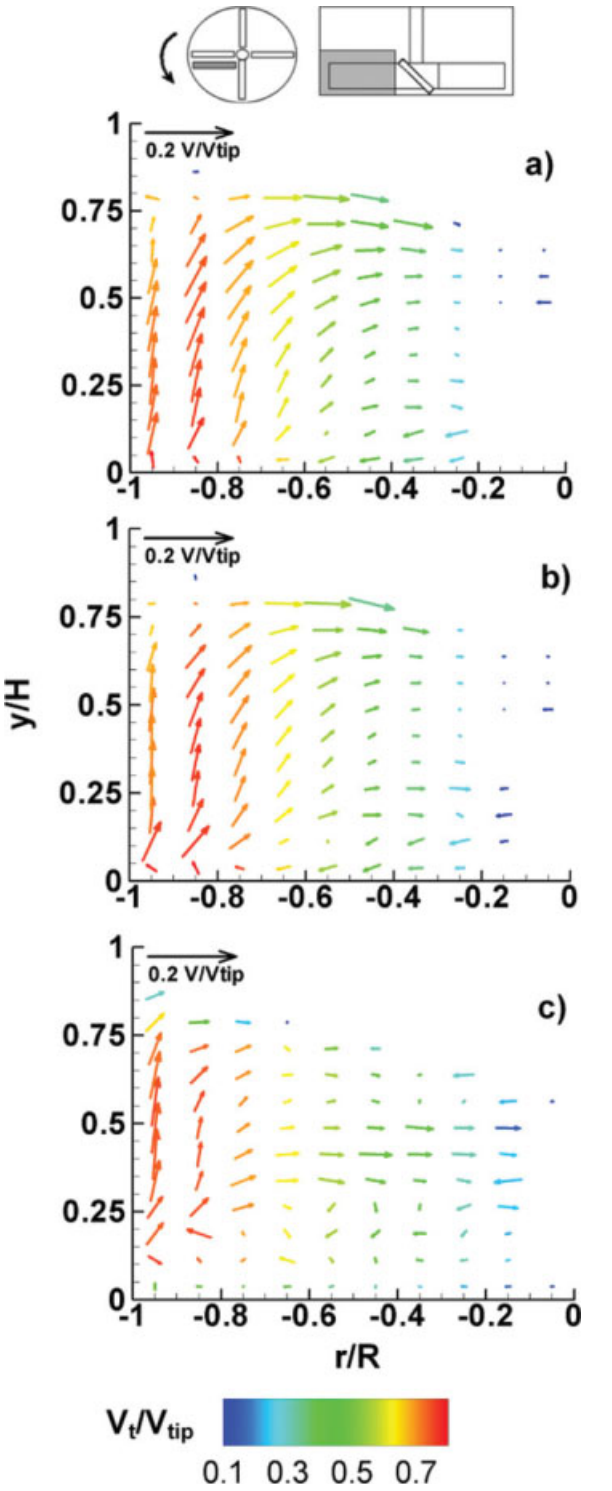

Figure 16. Velocity field in front of blade for different D/d.

(a) D/d = 94.5, b) D/d = 63.0 and c) D/d = 31.5. [Color figure can be viewed in the online issue, which is available at www.interscience.wiley.com.]

Figure 17 shows the effect of system size on mixing. As a result of the enhanced convective and diffusive particle transport, faster mixing kinetics are observed for the D/d >

Table 5. Effect of D/d on Normalized Particle Diffusivity and Peclet Number

D/d	$D_{\theta\theta}$*	D_{rr} *	D_{yy}*	$Pe_{\theta\theta}$	Pe_{rr}	Pe_{yy}
31.5	8.5×10^{-4}	3.3×10^{-4}	9.0×10^{-4}	720	152	70
63.0	1.3×10^{-3}	4.8×10^{-4}	2.2×10^{-3}	490	76	25
94.5	1.5×10^{-3}	5.9×10^{-4}	2.4×10^{-3}	400	56	23

31.5 cases. The degree of mixing is very similar in all three system sizes during the early stages of the mixing process. However, the RSD curve for the D/d = 31.5 case (Figure 17a) begins to level off after four revolutions, while the RSD values for the other cases continue to decrease. As can be seen from the top view snapshots shown in Figure 17b, the mixing process after five revolutions is down to the particle level for D/d = 63.0 and D/d = 94.5, while regions of unmixed particles still remain at D/d = 31.5. Little differences is observed between the mixing kinetics obtained at D/d = 63.0 and D/d = 94.5. Since a constant blade rotational speed was used for all mixer sizes, the tip speed of the blades increases with D/d in our simulations. However,

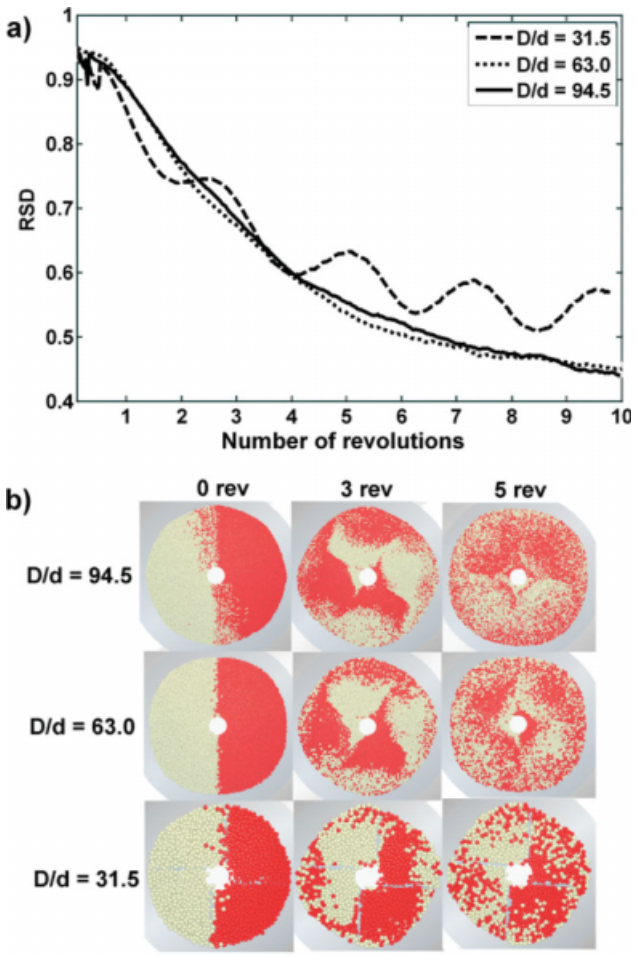

Figure 17. Effect of D/d on mixing.

(a) Relative standard deviation of the red particle concentration vs. number of revolutions, and (b) top view snapshots of mixing patterns for different D/d ratios. [Color figure can be viewed in the online issue, which is available at www.interscience.wiley.com.]

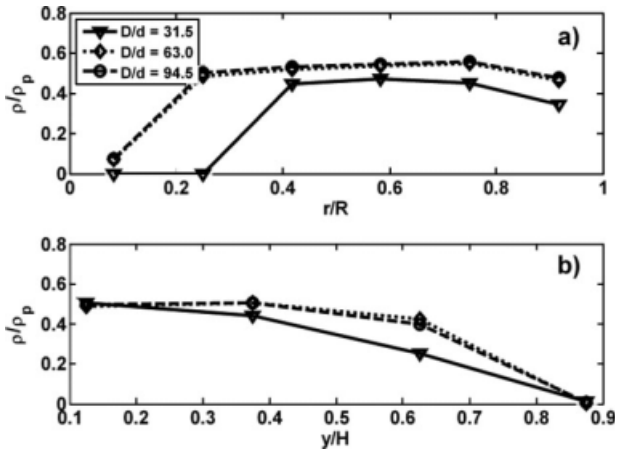

Figure 18. The effect of D/d on solids fraction.

(a) Solids fraction vs. r/R, and (b) solids fraction vs. y/H.

when the tip speed for the D/d = 63.0 case was set to that of the D/d = 31.5 and D/d = 94.0 cases, no difference in mixing was observed. These results imply that in the quasi-static regime, above a certain system size, the rotational speed of the blades provides the time scale for which the mixing process takes place. Further work is needed to investigate the effect of blade rotational speed on mixing kinetics when flow regime transition occurs.

Bed dilation is also affected by the D/d ratio. Figure 18 shows the time-averaged solids fraction ρ/ρ_p, where ρ is the bed bulk density during flow, and ρ_p is the density of the particles. The average solids fraction for the D/d = 31.5 case is roughly 40%, while at D/d > 31.5 a solids fraction of about 50% is observed. We hypothesize that the increase in bed dilation observed at the lower D/d ratio is a result of

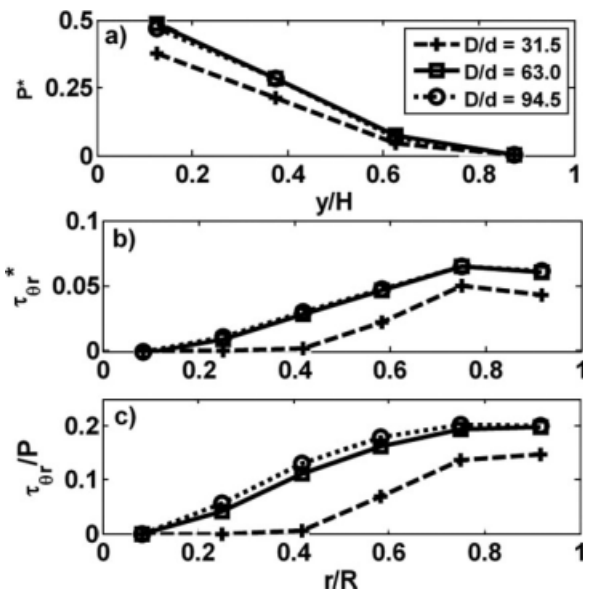

Figure 19. Scaled pressure, shear stress and bulk friction for different D/d ratios.

(a) Time-averaged pressure vs. y/H, and (b) Time averaged $\tau^*_{\theta r}$ vs. r/R and (c) Time averaged $\tau_{\theta r}/P$ vs. r/R.

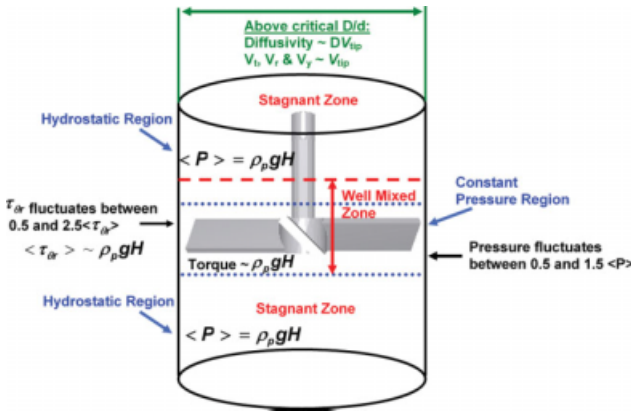

Figure 20. Scale-up of quasi-static flows in a bladed mixer with blades positioned below the surface of the particle bed.

[Color figure can be viewed in the online issue, which is available at www.interscience.wiley.com.]

the frictional contact chains that develop by the cylinder wall. As the blades rotate, the contact chains force material to move upward by the cylinder wall causing bed dilation. The maximum stable length of these contact chains is characterized by a certain number of particle diameters. The maximum number of particle diameters in a stable contact chain is a function of the system's frictional characteristics, but is independent of mixer size. As a result, the length of stable contact chains relative to the mixer diameter is larger at D/d = 31.5 causing the higher bed dilation.

We now look at the effect of system size on the stress profiles that develop inside the bladed mixer. We find that the time-averaged stresses increase as D/d is increased with the highest values obtained for the D/d = 94.5 case. The main reason for the increase in stresses is the increase in total weight of the particle bed at the higher D/d ratios (as the H/D ratio was kept constant in these simulations). Thus, we find that the normal and shear-stress values obtained at each D/d ratio can be scaled by the quantity $\rho_p gH$. Figure 19 shows the scaled pressure $P^* = P/\rho_p gH$, and shear-stress $\tau^*_{\theta r} = \tau_{\theta r}/\rho_p gH$ profiles, as well as the bulk-friction coefficient for the different D/d values. The pressure profiles obtained for all the D/d cases increase linearly with bed height (Figure 19a). The scaled pressure profile remains unchanged at D/d = 63.0 and D/d = 94.5, while a lower scaled pressure is obtained for the D/d = 31.5 case. The lower pressure is as a result of the increased bed dilation at this D/d ratio. It is interesting to note that the value of the scaled pressure at the bottom plate coincides with the average solids fraction at each D/d value. A similar behavior is observed for the scaled shear stress, (Figure 19b). While it is reasonable to expect that pressure would scale with the system's mass, we find that shear stress also scales with this quantity. Identical scaled shear stress values are obtained at the higher D/d ratios, while the D/d = 31.5 case is characterized by a lower scaled shear stress. This suggests that a larger amount of momentum is being transferred to the particle bed as a result of blade movement at the higher system sizes. The bulk-friction coefficients obtained show the same trend (Figure 19c) with higher values at D/d > 31.5. Note that even at the high D/d ratios, the resulting bulk-friction coefficient is lower than the value of the microscopic sliding friction coefficient ($\mu_s = 0.5$ in these simulations).

Our analysis suggest that, while different flow kinematics and stress profiles were obtained at the lower D/d ratio, scaling relationships exists for systems with D/d $\geq$ 63.0. In particular, our results suggest that there is a critical D/d system size, and that simple scaling relationships exist above this critical system size. Above the critical D/d system size, the following scaling relationships were observed. Mean velocity profiles, as well as velocity fluctuation amplitudes scale linearly with the blades' tip speed. Flow patterns are found to be independent of system size. Particle diffusivities scale linearly with system size and the blades' tip speed. Mixing kinetics are invariant of system size with the rotational speed dictating the mixing time scale. Bed dilation remains a constant as the system size is increased. The resulting pressure and shear-stress profiles scale linearly with the total weight of the particle bed. While further work is needed to verify that the obtained scaling relationships are still applicable at higher D/d ratios, the results presented here suggest that granular flows in bladed mixer could be scaled according to system size and operating conditions. The scaling relationships shown here are applicable to monodisperse, cohesionless spheres in the quasi-static regime. A more comprehensive study is needed to determine the effect of granular regime transition on the results presented here.

Conclusions

The discrete element method was used to analyze the effect of mixer properties and fill level on the observed granular behavior in bladed mixers. Fill level was demonstrated to influence granular flows in the bladed mixer. Higher convective and diffusive mixing was observed at the lower fill levels, with the best mixing performance obtained when the height of the particle bed just covers the top of the blades. While the mixing kinetics of the entire system were affected by fill level, it was found that bed dilation, and convective and diffusive mixing within the span of the blades remains invariant of fill level above a certain fill level (H/D > 0.32 in our simulations). Impeller torque was found to increase linearly with fill level. Time-averaged-pressure profiles were found to vary linearly with height at low-fill levels, and are approximated by a simple hydrostatic relationship. However, at high-fill levels, two regimes are obtained in the pressure profile. A hydrostatic region exists above the blades where pressure increases linearly with height, while a saturated region was obtained within the span of the blades where pressure is independent of blade height. The development of the saturated region was attributed to the 45° angle of the blades which cause the impeller to support the weight of the particles within the span of the blades. The saturated region is characterized by pressure and shear stress fluctuations with frequencies equal to the rotational speed of the blades. The amplitude of these fluctuations relative to the mean was found to be independent of fill level.

The frictional characteristics of the cylinder walls were shown to significantly affect flow patterns, particle diffusivities, mixing kinetics and shear stresses inside the mixer. At

low-particle-wall friction coefficients, secondary flow structures found in front of the blades at high-frictional conditions do not develop, thus, reducing convective mixing. High-particle-wall friction leads to an increase in particle diffusivity and diffusive mixing. Shear stresses inside the particle bed decrease with a decrease in cylinder wall friction. Blade position in the vertical direction was shown to affect flow patterns and granular temperature and shear stresses within the particle bed.

The effect of scaling up the mixer while keeping constant the particle diameter and the fill level was also studied. The system scale was quantified by taking the ratio of the mixer diameter to the particle diameter, D/d. Lower convective and diffusive mixing was observed for the lowest D/d ratio studied (D/d = 31.5), while enhanced mixing kinetics were obtained for the larger systems (D/d = 63.0 and 94.5). Bed dilation was highest for the D/d = 31.5 system, while a higher solids fraction was observed as mixer size was scaled-up. Normal and shear stress profiles were found to increase with mixer size. While different results were obtained at D/d = 31.5, the resulting granular behavior at D/d $\geq$ 63.0 was found to scale according to system size. The differences in behavior observed at D/d = 31.5 were attributed to the effect of wall friction, which is most prominent for smaller systems. Above a critical system size, the effect of wall friction is minimized and granular behavior could be predicted based on simple scaling relationships. Particle velocities and diffusivities vary linearly with the tip speed of the blades. The time-averaged solids fraction remains a constant. Additionally, the rotational speed of the blades provides the time scale in which the mixing process occurs. Normal and shear stresses were found to scale linearly with the total mass of the system and could be scaled by the quantity $\rho_p g H$.

Despite the complex behavior observed in bladed mixers, our results suggest that granular flows in these types of mixers can be scaled according to system size when the size of the mixer relative to the particle size is large enough to overcome wall effects. The simple scaling relationships obtained from our analysis are summarized in Figure 20 for quasi-static flows with a middle blade position. This configuration was chosen as it captures the important flow features at the different fill levels. Many questions remain unanswered regarding the effect of the parameters studied here in more complex granular systems such as polydisperse mixtures, nonspherical particle beds and cohesive systems. Further work is needed to verify whether the trends reported here are applicable to these systems.

Acknowledgments

B. Remy wishes to thank Bristol-Myers Squibb, Co. for financial support during an educational leave of absence. The authors would like to thank DEM Solutions for their support of this work. This work was partially supported by the National Science Foundation, the American Chemical Society Petroleum Research Fund, and the Engineering Research Center for Structured Organic Particulate Systems.

Notation

m_i = mass of particle i
R_i = radius of particle i
I_i = moment of inertial of particle i
v_i = velocity of particle i
g = acceleration due to gravity
F_{ij}^N = normal force resulting from the contact of particle i with particle j
F_{ij}^T = tangential force resulting from the contact of particle i with particle
$\tilde{k_n}$ = normal stiffness coefficient
$\tilde{k_t}$ = tangential stiffness coefficient
v_{rel}^t = relative tangential velocity of the colliding particles
E = Young's modulus
G = Shear modulus
R^* = effective radius of the colliding particles
e = coefficient of restitution
d = particle diameter
N = number of partilces in simulation
H = bed height prior to blade movement
D = diameter of mixer
R = radius of mixer
V^* = particle velocity normalized by the tip speed
V_{tip} = tip speed of blades
u'' = fluctuation velocity
T = granular temperature
D_{ij} = diffusion coefficient in the i direction due to a gradient in the j direction
Pe = Peclet number
U_i = average particle speed
V_c = control volume
P = pressure
$\langle P \rangle$ = temporal averaged pressure
M_{conc} = mean particle concentration
D/d = mixer diameter to particle diameter ratio
D_{ij}^* = normalized diffusion coefficient
P^* = normalized pressure

Greek letters

ω_i = angular velocity of particle i
τ_{rij} = torque resulting from the contact of particle i with particle j
δ_n = normal displacement
δ_t = tangential displacement
$\tilde{\gamma}_n$ = normal damping coefficient
$\tilde{\gamma}_t$ = tangential damping coefficient
σ = Poisson ratio
μ_r = rolling friction coefficient
μ_s = silding friction coefficient
ρ_p = particle density
ρ = bulk density during flow
τ_{ij} = stress on i plane in the j direction
$\langle \tau_{ij} \rangle$ = temporal averaged stress
μ_s^{p-p} = particle-particle sliding friction
μ_s^{p-w} = particle-cylinder wall sliding friction
σ_{conc} = standard deviation of particle concentration
τ_{ij}^* = normalized shear stress

Literature Cited

1. Muzzio FJ, Alexander A, Goodridge C, Shen E, Shinbrot T. *Solids Mixing Part A: Fundamentals of Solids Mixing*. In: Edward L. Paul VAA-O, Suzanne M. Kresta, ed. *Handbook of Industrial Mixing: Science and Practice*: John Wiley & Sons, Inc.; 2004:887–983.
2. Laurent BFC. Scaling factors in granular flow-analysis of experimental and simulations results. *Chem Eng Sci*. 2006;61(13):4138–4146.
3. Sinnott M, Cleary P. *3D DEM simulations of a high shear mixer*, 2006; Melbourne, Vic., Australia.
4. Gotoh K, Masuda H, Higashitani K. *Powder Technology Handbook*. Vol 10: ASM International; 2001.
5. Prescott JK. *Powder Handling*. In: Levin M, ed. Pharmaceutical Process Scale-up. Vol 118: Marcel Dekker; 2001:133–149.
6. Litster JD, Hapgood KP, Michaels JN, Sims A, Roberts M, Kameneni SK. Scale-up of mixer granulators for effective liquid distribution. *Powder Technol*. 2002;124(3):272–280.

7. Laurent BFC, Bridgwater J, Parker DJ. Motion in a particle bed agitated by a single blade. *AIChE J*. 2000;46(9):1723–1734.
8. Jones JR, Parker DJ, Bridgwater J. Axial mixing in a ploughshare mixer. *Powder Technol*. 2007;178(2):73–86.
9. Tardos GI, Hapgood KP, Ipadeola OO, Michaels JN. Stress measurements in high-shear granulators using calibrated "test" particles: application to scale-up. *Powder Technol*. 2004;140(3):217–227.
10. Lekhal A, Conway SL, Glasser BJ, Khinast JG. Characterization of granular flow of wet solids in a bladed mixer. *AIChE J*. 2006; 52(8):2757–2766.
11. Conway SL, Lekhal A, Khinast JG, Glasser BJ. Granular flow and segregation in a four-bladed mixer. *Chem Eng Sci*. 2005/12 2005; 60(24):7091–7107.
12. Stewart RL, Bridgwater J, Parker DJ. Granular flow over a flat-bladed stirrer. *Chem Eng Sci*. 2001;56(14):4257–4271.
13. Sato Y, Nakamura H, Watano S. Numerical analysis of agitation torque and particle motion in a high shear mixer. *Powder Technol*. 2008;186(2):130–136.
14. Remy B, Khinast JG, Glasser BJ. Discrete element simulation of free flowing grains in a four-bladed mixer. *AIChE J*. 2009; 55(8):2035–2048.
15. Zhou YC, Yu AB, Stewart RL, Bridgwater J. Microdynamic analysis of the particle flow in a cylindrical bladed mixer. *Chem Eng Sci*. 2004/3 2004;59(6):1343–1364.
16. Zhou YC, Yu AB, Bridgwater J. Segregation of binary mixture of particles in a bladed mixer. *J Chem Technol Biotechnol*. 2003;78(2-3):187–193.
17. Stewart RL, Bridgwater J, Zhou YC, Yu AB. Simulated and measured flow of granules in a bladed mixer--a detailed comparison. *Chem Eng Sci*. 2001;56(19):5457–5471.
18. Gyenis J, Ulbert Z, Szépvölgyi J, Tsuji Y. Discrete particle simulation of flow regimes in bulk solids mixing and conveying. *Powder Technol*. 1999;104(3):248–257.
19. Bertrand F, Leclaire LA, Levecque G. DEM-based models for the mixing of granular materials. *Chem Eng Sci*. 2005;60(8-9 SPEC ISS):2517–2531.
20. Chung YC, Ooi JY. Influence of discrete element model parameters on bulk behavior of a granular solid under confined compression. *Part Sci Technol*. 2008;26(1):83–96.
21. Limtrakul S, Boonsrirat A, Vatanatham T. DEM modeling and simulation of a catalytic gas-solid fluidized bed reactor: a spouted bed as a case study. *Chem Eng Sci*. 2004;59(22-23):5225–5231.
22. Limtrakul S, Chalermwattanatai A, Unggurawirote K, Tsuji Y, Kawaguchi T, Tanthapanichakoon W. Discrete particle simulation of solids motion in a gas-solid fluidized bed. *Chem Eng Sci*. 2003;58(3-6):915–921.
23. Lemieux M, Leonard G, Doucet J et al. Large-scale numerical investigation of solids mixing in a V-blender using the discrete element method. *Powder Technol*. 2008;181(2):205–216.
24. Ottino JM, Khakhar DV. Scaling of granular flow processes: From surface flows to design rules. *AIChE J*. 2002;48(10):2157–2166.
25. Ding YL, Forster RN, Seville JPK, Parker DJ. Scaling relationships for rotating drums. *Chem Eng Sci*. 2001;56(12):3737–3750.
26. Felix G, Falk V, D'Ortona U. Granular flows in a rotating drum: the scaling law between velocity and thickness of the flow. *Eur Phys J E*. 2007;22(1):25–31.
27. Tsuji Y, Tanaka T, Ishida T. Lagrangian numerical simulation of plug flow of cohesionless particles in a horizontal pipe. *Powder Technol*. 1992;71(3):239–250.
28. Ford KJ. *Experimental Investigation of Phase Behavior and the Dynamics of Vertically Vibrated Deep Granular Beds*. Chemical Engineering, Lehigh University; 2008.
29. Campbell CS. Self-diffusion in granular shear flows. *J Fluid Mech*. 25 April 1997 1997;348:85–101.
30. Campbell CS. Granular shear flows at the elastic limit. *J Fluid Mech*. 2002;465:261–291.
31. Glasser BJ, Goldhirsch I. Scale dependence, correlations, and fluctuations of stresses in rapid granular flows. *Phys Fluids*. 2001;13(2):407–420.
32. Sperl M. Experiments on corn pressure in silo cells - Translation and comment of Janssen's paper from 1895. *Granular Matter*. 2006;8(2):59–65.
33. Duran J. *The static properties of a granular pile*. In: Lam L, Langevin D, eds. *Sands, Powders and Grains*. 1st ed. New York: Springer; 1999: 54–75.
34. Bertho Y, Giorgiutti-Dauphine F, Hulin JP. Dynamical Janssen effect on granular packing with moving walls. *Phys Rev Lett*. 2003; 90(14):144301–144301.
35. Watano S, Okamoto T, Sato Y, Osako Y. Scale-up of high shear granulation based on the internal stress measurement. *Chem Pharm Bull*. 2005;53(4):351–354.
36. Masson S, Martinez J. Effect of particle mechanical properties on silo flow and stresses from distinct element simulations. *Powder Technol*. 2000;109(1):164–178.
37. Taberlet N, Richard P, Delannay R. The effect of sidewall friction on dense granular flows. *Comput Math Appl*. 2008;55(2):230–234.
38. Jaehyuk C, Kudrolli A, Rosales RR, Bazant MZ. Diffusion and mixing in gravity-driven dense granular flows. *Phys Rev Lett*. 2004;92(17):174301–174301.

Manuscript received Dec. 2, 2008, revision received Mar. 30, 2009, and final revision received May 22, 2009.